ARTICLES
https://doi.org/10.1038/s41557-018-0002-2
nature chemistry

Chemical evolution of atmospheric organic carbon over multiple generations of oxidation

Gabriel Isaacman-VanWertz[1,2*], Paola Massoli[3], Rachel O'Brien[1], Christopher Lim[1], Jonathan P. Franklin[1], Joshua A. Moss[1], James F. Hunter[1], John B. Nowak[3,4], Manjula R. Canagaratna[3], Pawel K. Misztal[5], Caleb Arata[5], Joseph R. Roscioli[3], Scott T. Herndon[3], Timothy B. Onasch[3], Andrew T. Lambe[3], John T. Jayne[3], Luping Su[6], Daniel A. Knopf[6], Allen H. Goldstein[5], Douglas R. Worsnop[3] and Jesse H. Kroll[1,7*]

The evolution of atmospheric organic carbon as it undergoes oxidation has a controlling influence on concentrations of key atmospheric species, including particulate matter, ozone and oxidants. However, full characterization of organic carbon over hours to days of atmospheric processing has been stymied by its extreme chemical complexity. Here we study the multigenerational oxidation of α-pinene in the laboratory, characterizing products with several state-of-the-art analytical techniques. Although quantification of some early generation products remains elusive, full carbon closure is achieved (within measurement uncertainty) by the end of the experiments. These results provide new insights into the effects of oxidation on organic carbon properties (volatility, oxidation state and reactivity) and the atmospheric lifecycle of organic carbon. Following an initial period characterized by functionalization reactions and particle growth, fragmentation reactions dominate, forming smaller species. After approximately one day of atmospheric aging, most carbon is sequestered in two long-lived reservoirs—volatile oxidized gases and low-volatility particulate matter.

Organic compounds play a central role in the chemistry of the atmosphere by contributing to ozone formation[1,2], serving as the primary sink for oxidants in the atmosphere[3,4] and constituting a substantial fraction of global submicrometre particulate matter[5,6]. Organic carbon (OC) enters the atmosphere primarily as high-volatility gases. Oxidation of these compounds yields a large number of products, including organic species in the gas phase (gas-phase OC, gOC), organic species in the condensed phase (particle-phase OC, pOC) and inorganic carbon-containing species (CO and CO_2). All of these products (other than CO_2) may themselves undergo further oxidation, continuing this process over multiple generations to produce a highly complex, chemically dynamic mixture of compounds that spans a wide range in chemical composition and properties (for example, volatility)[7–11]. Oxidation continues until OC is either converted to CO_2 or removed from the atmosphere through deposition to the Earth's surface, thereby transporting a wide range of organic compounds into other components of the Earth system. Our ability to track the oxidative evolution of OC over its entire atmospheric lifetime therefore controls our ability not only to understand critical issues in air quality and atmospheric chemistry, but ultimately to understand the impacts of organic emissions on human health, ecosystems and Earth's climate.

The comprehensive measurement of all oxidation products from a given chemical system has been elusive due to the analytical challenges associated with detecting, characterizing and quantifying compounds within complex organic mixtures. Only studies of the simplest organic compounds have achieved 'carbon closure', fully characterizing the product mixture throughout oxidation[12]. For larger species, a large fraction of the products has remained unmeasured and/or uncharacterized, even in the early stages of reaction (first one or two generations of oxidation)[13,14]. As a result, there is substantial uncertainty as to the fate and impact of OC over timescales longer than several hours after emission. For example, the possibility of substantial unmeasured 'pools' of OC has major implications for the formation of particle-phase mass through the gas-to-particle partitioning of condensable gases. It has traditionally been assumed that such unmeasured carbon will not condense to contribute to particle-phase mass. However, if instead unmeasured carbon in laboratory experiments is irreversibly lost to chamber walls via vapour deposition[15] or reacts over multiple generations to form lower-volatility gases[9,16], then formation of pOC from many precursors may be substantially higher than currently estimated. The properties and reactivity of organic oxidation products formed over multiple generations will also impact ozone production, removal pathways (for example, wet and dry deposition) of pollutants, and reactivity and cycling of oxidants. A quantitative, predictive description of these processes across spatial scales therefore relies critically on the measurement of the chemistry of such species, and more generally on our ability to measure and track all OC in a reactive system.

Here, we apply recent advances in analytical instrumentation to characterize the full mixture of products formed in hydrocarbon oxidation with the goal of achieving carbon closure, enabling a more complete understanding of the chemical properties and transformation processes of atmospheric OC. We access the entire

[1]Department of Civil and Environmental Engineering, Massachusetts Institute of Technology, Cambridge, MA, USA. [2]Department of Civil and Environmental Engineering, Virginia Tech, Blacksburg, VA, USA. [3]Aerodyne Research Inc., Billerica, MA, USA. [4]NASA Langley Research Center, Hampton, VA, USA. [5]Department of Environmental Science, Policy, and Management, University of California, Berkeley, Berkeley, CA, USA. [6]School of Marine and Atmospheric Sciences, Stony Brook University, Stony Brook, NY, USA. [7]Department of Chemical Engineering, Massachusetts Institute of Technology, Cambridge, MA, USA. *e-mail: ivw@vt.edu; jhkroll@mit.edu

range of expected chemical properties of suspended products[17] with an array of state-of-the-art analytical instruments: a thermodenuder aerosol mass spectrometer[18] (TD-AMS) and scanning mobility particle sizer (SMPS) to measure pOC with volatility resolution, a proton transfer reaction mass spectrometer[19,20] (PTR-MS) and two chemical ionization mass spectrometers[21] (I^- CIMS and NO_3^- CIMS[22–25]) to measure gOC, and two tunable infrared laser differential absorption spectrometers (TILDAS) to measure C_1 compounds (CO, formaldehyde and formic acid). We combine the data from these instruments to present a unified, time-resolved description of the chemical composition of two oxidation systems: initial oxidation of α-pinene (a monoterpene) through photooxidation by hydroxyl radicals (OH) in the presence of NO, and ozonolysis in the absence of NO, followed in both cases by continued high-NO OH oxidation. All experiments were performed at 20 °C and low relative humidity (<5%); see Methods and Supplementary Section 1 for details on reaction conditions and instrument operation, calibration and uncertainty. These systems were chosen because their initial chemistry has been subject to extensive theoretical and experimental characterization[26–28], though the subsequent multigenerational oxidation ('aging') of the reaction mixture (particularly gOC) has received substantially less study[29]. By the end of the experiments, all carbon is measured to within experimental uncertainties, enabling a coherent and detailed picture of the chemical evolution of the product mixture, and providing new insights into the lifecycle and fate of atmospheric OC.

Results

Carbon closure. All products measured in the OH-initiated oxidation of α-pinene are shown in Fig. 1. Results are qualitatively similar to those in the ozonolysis experiment, so ozonolysis results are given in Supplementary Section 5. Initial reaction of α-pinene is immediately accompanied by a concomitant increase in both gOC and pOC oxidation products. Particle-phase OC is formed in the first generations of oxidation, with only minor additional formation after the α-pinene is fully consumed, and accounts for 14 ± 3% of the total carbon by the end of the experiment (~24 h of equivalent daytime atmospheric oxidation). We focus our characterization of pOC on average chemical properties and volatility distributions, providing an ensemble description of the aerosol, while composition of gOC is characterized by individual species. Identified gas-phase products are CO, formaldehyde, formic acid, acetic acid, acetone and pinonaldehyde. Concentrations of each identified product vary over the course of the experiment, but in total account for 41 ± 5% of the carbon by the end. CO_2 is not measured here but is expected to be similar in concentration to CO (~4%)[30].

In addition to known compounds, chemical species measured include a large number of 'unidentified' gas-phase reaction products, detected by the gas-phase mass spectrometers as 310 ions. Structures for these ions cannot be unambiguously assigned, but molecular formulas are known, from which chemical properties (for example, volatility) can be estimated using group contribution methods[31]. These unidentified species comprise 46 ± 17% of the carbon at the end of the experiment, most of which is measured by PTR-MS and I^- CIMS. Species measured by the NO_3^- CIMS (extremely low volatility, highly oxidized gases)[32] account for <0.5% of the total carbon, and so are not included in Fig. 1. The overlap between carbon measured by each instrument is minor, with ions of the same formulas measured by different instruments accounting for less than 20 ppb C (4% of carbon, see Methods). The dominant single contributor to unidentified carbon is $C_3H_4O_4$ (yield of ~5%, measured by I^- CIMS), which has previously been observed in the atmosphere and identified as malonic acid[33]; however, its ion cluster strength (Supplementary Fig. 1) indicates that it is not malonic acid but rather some isomer (or combination of isomers) thereof (for example, the modelled pinene oxidation product 3-oxo-peroxypropanoic acid[34]). This highlights the need for new measurements that provide information on molecular structure and improved characterization of these unidentified species[35]. Online measurements, such as the ones used here, typically provide only chemical formulas; offline techniques (for example, tandem mass spectrometry), on the other hand, tend not to be adapted for the direct, real-time analysis of these gas-phase compounds, and may induce chemical transformations on collection or extraction.

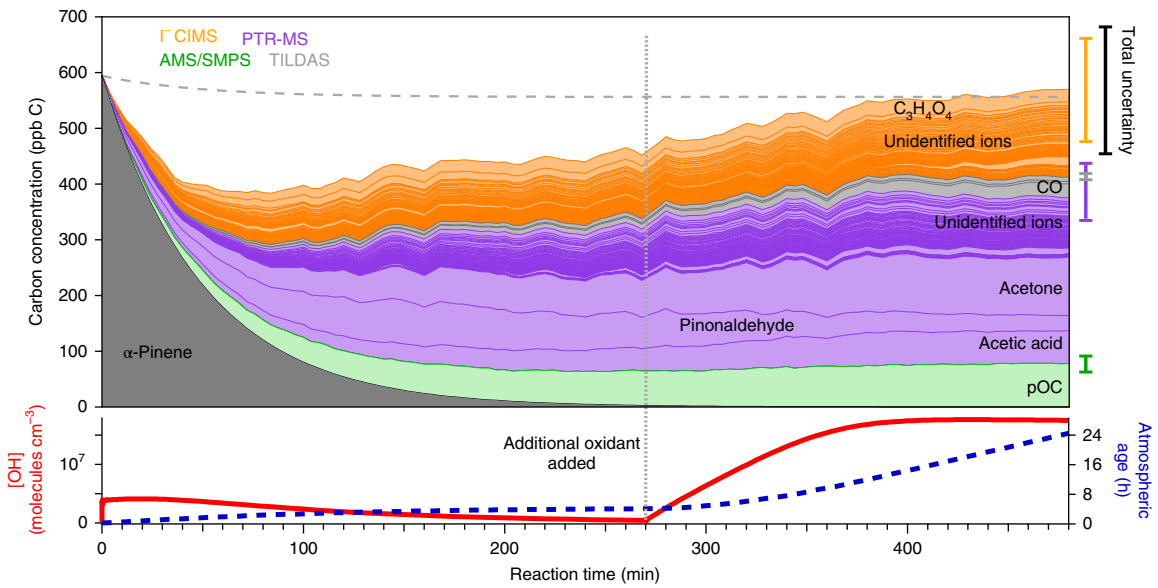

Fig. 1 | Measured carbon in the photooxidation of α-pinene, characterized by molecular formula. Each product ion of α-pinene (dark grey) is coloured by the instrument by which it was measured. Unlabelled species measured by TILDAS are formic acid and formaldehyde. The uncertainty range for each instrument is shown on the right. Carbon closure (denoted by the grey dashed line, which accounts for dilution of the precursor) is achieved within measurement uncertainty (102 ± 20%), providing an unprecedented opportunity to study the complete chemical evolution of atmospheric oxidation processes. All concentrations are corrected for dilution; pOC is also corrected for particle deposition to the chamber walls. Bottom: modelled OH concentration (red line) and approximate photochemical age in the atmosphere (blue dashed line), assuming an average atmospheric OH concentration of 2×10^6 molecules cm^{-3}. The corresponding plot for the α-pinene ozonolysis experiment is given in Supplementary Fig. 10.

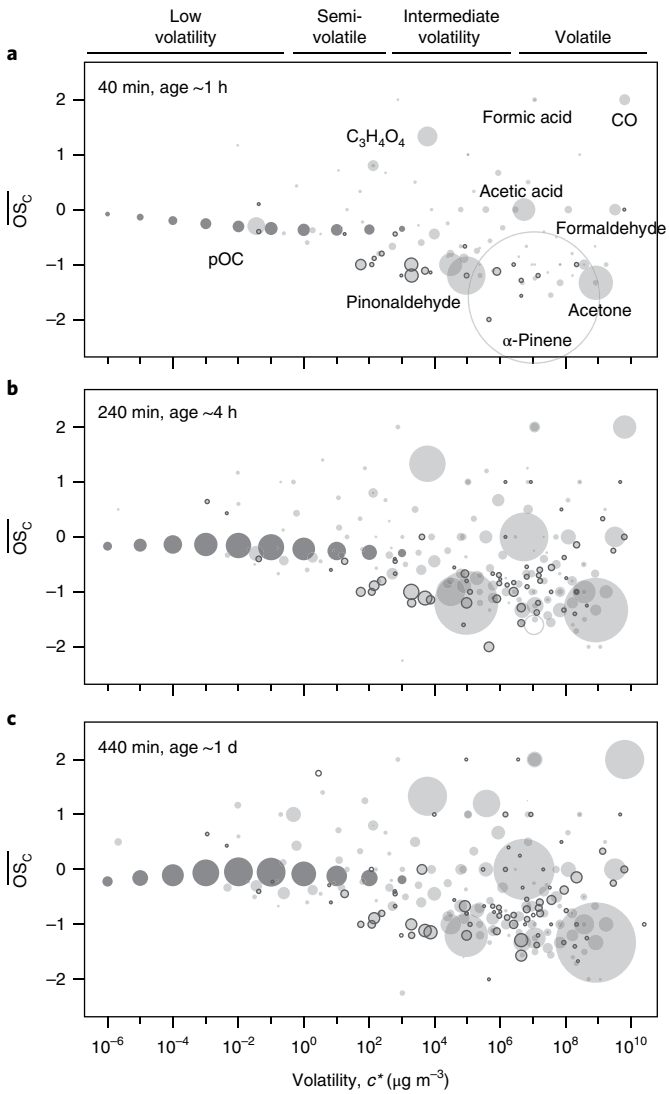

Fig. 2 | Chemical characterization of carbon measured in the photooxidation of α-pinene in terms of $\overline{OS_C}$ and c^*, commonly used for simplified representation of atmospheric organic carbon. a–c, These measurements illustrate the highly dynamic nature of the chemical system. Circle area is proportional to carbon concentration. Hollow circle, α-pinene; light grey, gas-phase species; dark grey, pOC. Data shown are for the average $\overline{OS_C}$ of each volatility bin measured by TD-AMS. Gas-phase species containing nitrate groups (defined as containing nitrogen and ≥3 oxygen atoms) are outlined. Distributions are provided after approximately 1 h (**a**), 4 h (**b**) and 24 h (**c**) of equivalent atmospheric age. Some products are observed to increase in concentration throughout the experiment (for example, CO), while others form and are then depleted (for example, pinonaldehyde), demonstrating that differences in reactivity and lifetime drive the dominant formation of less-reactive products. The full time evolution of these data is available in Supplementary Videos 1 and 2.

The total measured carbon yield is 102 ± 20% (1σ) by the end of the experiment. Calibrations of individual ions are relatively uncertain (for example, a factor of 2.5 per ion in the I$^-$ CIMS) because authentic standards are not available for most species. However, uncertainties in each ion are primarily due to random deviations from average calibration relationships rather than systematic bias; relative uncertainty for total measured carbon is therefore lower than that for any given ion and is calculated by the quadrature addition of individual absolute uncertainties. The contributions of each instrument to total uncertainty is provided in the Methods, and given in detail in Supplementary Table 1. 'Carbon closure' is achieved in this experiment within measurement uncertainty, allowing for a more comprehensive characterization of the evolving carbon distribution over these timescales than previously possible. This also indicates that the loss of condensable carbon to chamber walls or other surfaces is not a major sink for reaction products in this experiment, as expected given the fast rate of oxidation and the use of seed particles as a condensation sink[36–38], and supported by modelled gas–particle–wall partitioning (Supplementary Section 4).

Not all carbon is measured throughout the entire experiment; some 'missing' carbon (up to ~40%) is unmeasured early in the experiment. The time dependence of this unmeasured carbon suggests it is made up of early-generation products that quickly react away (with a ~4 h timescale) to yield measured products, leading to the observed carbon closure by the end of the experiment. These unmeasured species may be compounds that are not readily detected by the instrument suite. For example, the one peak in the I$^-$ CIMS mass spectrum that is above the detection limit but substantially below the threshold for reliable instrument calibration (and hence not included in Fig. 1) is $C_{10}H_{17}NO_4$ (Supplementary Fig. 2). This likely corresponds to α-pinene hydroxynitrate, a first-generation oxidation product known to be formed in high yields (~15%), but that is not sensitively measured by any of the present instruments[27,39]. Importantly, the temporal behaviour and ion intensity of this species (after applying an approximate calibration factor[40]) matches the unmeasured carbon well (Supplementary Section 4). 'Missing' carbon is also observed in the ozonolysis experiment (Supplementary Section 5), for which no nitrate formation is expected, so it appears that this instrument suite is not generally sensitive to lightly oxidized, lower-volatility gases, leading to poor carbon closure in the early generations of oxidation. In addition to undetected or poorly detected ions, unmeasured carbon may include underestimation of low-sensitivity isomers of detected ions, which is particularly likely for isomers of lightly functionalized ions (Supplementary Section 2). Early-generation compounds, comprising gases of relatively low volatility, may also reversibly partition to reactor or inlet walls[41] and re-volatilize on reaction of their gas-phase component with OH, which could also contribute to unmeasured carbon early in the experiment. Thus, despite uncertainties related to its molecular identity, the unmeasured carbon likely comprises lightly oxidized, relatively low-volatility gas-phase products. Indeed, this unmeasured carbon correlates well with the least-oxygenated measured ions (Supplementary Fig. 4). Moreover, the majority of the OC (and all of it by the end of the experiment) is quantified and characterized by chemical properties and formulas, providing a unique opportunity to examine the evolution of the composition and chemistry of OC over multiple generations of oxidation.

Evolving properties of the carbon. The changing composition of this complex mixture with oxidation is shown in Fig. 2, as three 'snapshots' of the product distribution in terms of carbon oxidation state ($\overline{OS_C}$) versus volatility (expressed as saturation concentration, c^*), often referred to as the 'two-dimensional volatility basis set'[10,42]. In the first hour of the experiment (Fig. 2a), carbon is dominated by the precursor, α-pinene, and the formation of products with intermediate volatility ($c^* = 10^3$–10^6 μg m^{-3}), as well as some higher-volatility gases (for example, acetone, acetic acid), and particle-phase mass. By the end of the initial oxidation, after nearly all α-pinene has reacted (Fig. 2b), the product mixture spans a wide range of volatilities and oxidation states. On further oxidation (Fig. 2c), the distribution of products changes further, indicating the importance of continuing oxidation chemistry beyond the initial α-pinene oxidation.

In this chemically dynamic system, the behaviour of different products is determined by both their formation pathways and their lifetime versus further oxidation by OH. Some early-generation products,

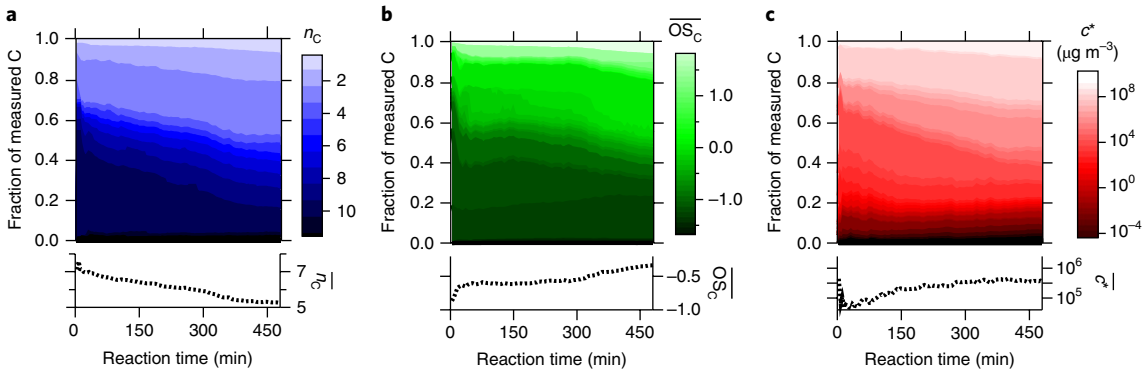

Fig. 3 | Distribution of key chemical properties of gas- and particle-phase products during the photooxidation of α-pinene. **a**, Number of carbon atoms, n_C. **b**, Oxidation state of carbon, $\overline{OS_C}$. **c**, Volatility in terms of saturation concentration, c^*. Each property is denoted by the colour scale shown. The properties of only the measured oxidation products (and not of the α-pinene precursor or the 'unmeasured' carbon) are shown; the plots in which α-pinene is included are provided in Supplementary Fig. 6. Bottom: evolution of carbon-weighted averages of each property demonstrate several general trends in atmospheric oxidation: initial formation of pOC and lightly oxygenated moderately volatile products, followed by fragmentation of gases to yield small oxygenated compounds.

including most intermediate-volatility organic compounds (IVOCs; for example, pinonaldehyde and multifunctional nitrates), exhibit rapid decreases in concentration after formation, consistent with their high reactivity[43,44]. In contrast, concentrations of some of the volatile compounds (for example, CO and acetone) consistently increase throughout the experiment. These are formed both from the initial oxidation of α-pinene as well as from the multigenerational oxidation of reaction products, and their slow reaction rates with OH preclude any significant decay over the timescales of the experiment. This category of less-reactive products also includes pOC, which increases throughout the experiment with only relatively minor changes in average properties, consistent with the long lifetime of particulate carbon against heterogeneous oxidation by gas-phase oxidants[45,46].

The evolution of the organic mixture as a whole can be described in terms of changes to key chemical properties of the measured products. Figure 3 shows the evolving distributions of three such properties: carbon number (n_C), $\overline{OS_C}$ and c^*. The n_C of observed products (Fig. 3a) exhibits a clear and dramatic change with oxidation: C_{10} species make up a large fraction (~50%, probably an underestimate as the early-generation unmeasured species are expected to be C_{10}), indicating the importance of functionalization reactions (addition of oxygen-containing groups) early in the reaction. These reactions contribute to the early formation of pOC via gas-to-particle conversion and in-particle accretion reactions that yield low volatility products. However, trends in chemical properties are dominated by gOC, which is the majority fraction of carbon. (The individual trends for pOC and gOC are shown in Supplementary Fig. 6). Further oxidation depletes gas-phase C_{10} compounds, which account for only 12% of the carbon by the end of the experiment. Their oxidation produces species with smaller carbon numbers (in particular C_{1-3}), suggesting that later-generation oxidation is dominated by fragmentation reactions. The $\overline{OS_C}$ distribution of the product mixture (Fig. 3b) is initially dominated by species with low (<-0.5) oxidation states, but further oxidation leads to the formation of higher-oxidation-state products, including very oxidized products with oxidation state $>+1$ (for example, formic acid and CO) and a few less-oxidized species (mostly acetone).

The volatility distribution (Fig. 3c) also undergoes major changes with oxidation. Initial product carbon is dominated by gas-phase IVOCs, C_{10} products formed by the addition of one to three functional groups to the carbon skeleton of the precursor. An early drop in volatility is observed because initially formed products include low-volatility pOC, which is measured, and intermediate-volatility gOC, which is partly unmeasured. As gas-phase species oxidize, the distribution of volatilities shifts away from IVOCs towards both higher- and lower-volatility products. By the end of the experiment, IVOCs represent a small fraction of the total carbon, which is instead dominated by high-volatility gases (formed from fragmentation reactions) or pOC (formed mostly from functionalization reactions). The trends observed in Fig. 3 are further enhanced by including α-pinene (Supplementary Fig. 6) or unmeasured species, as those have chemical properties similar to early-generation products (large, moderately volatile and lightly oxidized). The ozonolysis experiment exhibits the same trends as the photooxidation, but with fewer changes during the initial oxidation, since the initial reaction ceases after the oxidation of the double bonds.

The evolution of the organic mixture, in which the early-generation species (mostly large, lightly oxidized, intermediate-volatility species) react to form small, volatile species in the gas phase and low-volatility species in the particle phase, has important implications for the evolving reactivity and lifetime of atmospheric OC. Figure 4a shows the changes to the distribution of the atmospheric lifetime against reaction with OH (τ_{ox}) of the product mixture. Functionalized IVOCs generally have lifetimes of only 3–9 h, so the lifetimes of initial products are generally short[45]. Unmeasured carbon, representing one or a distribution of several such compounds, is included in Fig. 4 with a lifetime of the observed decay timescale (~4 h, time dependence of unmeasured mass shown in Supplementary Fig. 9).

While the initial IVOC products are short lived with respect to oxidation, other products are extremely long-lived, such as CO ($\tau_{ox}=39$ d; ref. [47]), acetone ($\tau_{ox}=34$ d; ref. [48]) and pOC ($\tau_{ox}=69$ d; ref. [46]). Over the course of the experiment, the IVOCs react away and these longer-lived species continue to increase in concentration, increasing the average lifetime of products in the mixture from 5 h to 2 d. By the end of the experiment, more than half of the carbon is in species that are sufficiently long-lived ($\tau_{ox}>20$ h) to be unreactive on the timescale of the experiment. This tendency towards long-lived species is a natural consequence of any multigenerational reaction system, as less-reactive products represent 'kinetic bottlenecks' and hence will necessarily accumulate. Reversible deposition to walls may impact the timescale of the reaction in this study by temporarily sequestering some reactive carbon from oxidation by OH, but these processes will not substantially diminish the kinetic tendency towards less-reactive products. In the present system, this tendency is closely correlated with the evolving volatility distributions, as long-lived species tend to be either small gas-phase oxygenates (for example, CO, acetone) or present in the condensed phase (as pOC). Thus, within approximately

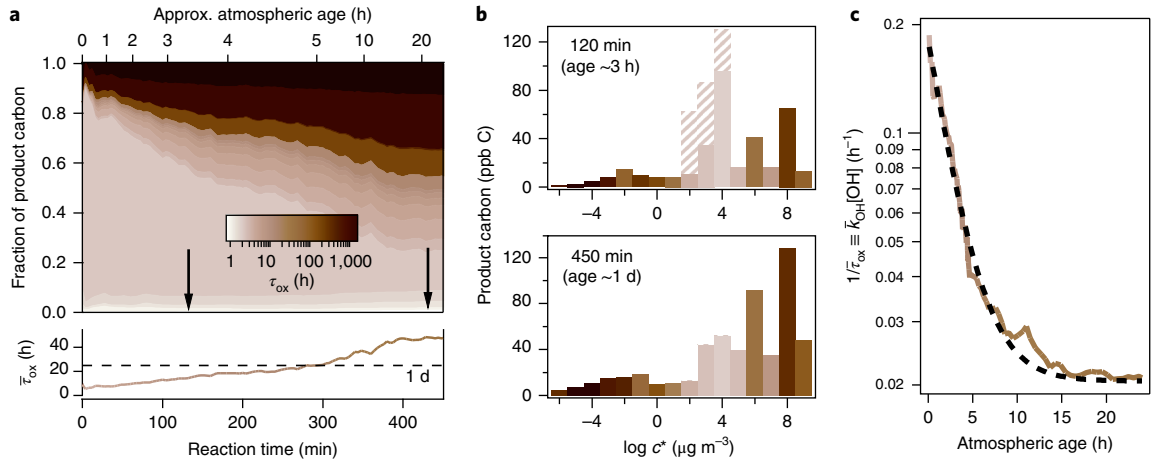

Fig. 4 | Changes in atmospheric lifetime and reactivity through multigenerational oxidation of α-pinene. a, Time-dependent distribution of atmospheric lifetime against oxidation by OH (τ_{ox}) including unmeasured carbon (for which $\tau_{ox} = 4$ h is assumed). Average trend is shown in the bottom panel. **b**, The volatility distribution of carbon at two points in the experiment. Times shown are denoted by arrows in **a**: relatively early (top) and late (bottom) in the reaction. Volatility bins are coloured by τ_{ox} with the same colour scale as in **a**. Unmeasured carbon is assumed to be distributed evenly across $c^* = 10^2$–10^4 μg m^{-3} (hashed bars) for illustrative purposes. **c**, Carbon-weighted average OH reactivity (assuming average OH concentration of 2×10^6 molecules cm^{-3}). Exponential fit has a decay constant, $\tau_{\overline{k_{OH}}}$, of 2.8 h (black dashed line). The average observed trend of increasing lifetime is shown to lead to the sequestration of carbon into high- and low-volatility reservoirs of low-reactivity carbon (small oxygenated gases and pOC, respectively) and a rapid decrease in overall reactivity.

1 d of atmospheric aging of this system, the volatility distribution of the product mixture becomes bimodal, dominated by particles and long-lived high-volatility gases (Fig. 4b). This decrease in reactivity through sequestration of carbon in 'low-reactivity pools' occurs roughly exponentially, with a characteristic time of ~3 h (Fig. 4c); this timescale matches the approximate lifetime of the first-generation products that drive the initial reactivity of the product mixture. Chemical systems are expected to vary in their timescales and composition depending on reaction rates of reactants and products, and the impacts of other chemical processes (for example, aqueous and multiphase reactions), but the tendency towards long-lived products is expected for most atmospheric systems.

Discussion

By characterizing nearly all the products formed in a complex chemical system in terms of their molecular formulas and physicochemical properties, we have been able to examine the products and evolution of atmospheric OC through multigenerational oxidation. Initial oxidation occurs through the addition of functional groups to form pOC mass and large, intermediate-volatility gases, but upon further oxidation, gas-phase products quickly fragment into high-volatility compounds. Particulate carbon and some oxidized volatile gases are resistant to further oxidation by OH, so carbon effectively becomes sequestered in these two pools. The present results are limited to the oxidation of a single precursor hydrocarbon, under a limited set of reaction conditions, and other chemical systems may exhibit different behaviour. However, known long-lived products (for example, pOC, formic acid, CO and so on) are formed by a wide range of oxidation systems, and longer-lived species will necessarily accumulate over the course of multiple generations of oxidation. Thus the general trends shown in Fig. 4—the eventual decrease in reactivity and the bifurcation in volatility—are likely to be common features of the oxidation of most atmospheric organic species. Ambient processes that are not captured by these experiments (for example, aqueous-phase reactions, in-particle secondary chemistry[49], reactive uptake of soluble gases such as those formed from isoprene oxidation[50,51]) may increase the oxidation or fragmentation of pOC or alter chemical pathways. This would shift the relative balance between condensed-phase and high-volatility long-lived reservoirs, but is unlikely to substantially increase or change the trend in the overall reactivity of OC.

The observed timescale for oxidative removal of reactive gases and formation of long-lived species has broad implications for understanding the fate of atmospheric OC on global and regional scales. Near emission sources, the diverse and complex mixture of functionalized gases formed from emissions are likely to comprise a significant fraction of suspended carbon, playing a critical role in particle growth, OH reactivity and depositional loss[11,16,52–56]. However, farther from emissions, IVOCs will be substantially depleted and most carbon will be found in relatively few long-lived constituents, so composition and removal of OC in remote regions will be dominated by particles and C_{1-3} gases. Where an air mass is on the continuum between near- and far-field is a function of both the inherent timescales for oxidation of a given chemical system and the 'average age' of the OC. Some approaches to quantify the average age of an air mass have been developed, but are generally limited to anthropogenically influenced chemistries[57,58]. The fate of atmospheric OC is determined by the competition between the oxidation reactions studied, other chemical processes (for example, aqueous-phase reactions) that may modify the oxidation pathways, and deposition. The relative timescales of each govern the extent to which emitted carbon is deposited as lightly functionalized species before being sequestered by oxidation. The timescales of oxidation measured in this work therefore need to be complemented by better observational constraints on average age of OC and timescales of removal to improve understanding of the lifecycle and fate of OC under a range of atmospheric conditions.

Methods

Reaction conditions. Studies were carried out using a fixed-volume temperature-controlled 7.5 m^3 Teflon environmental chamber, in which α-pinene (60 ppb), ammonium sulfate aerosol (~70 μg m^{-3}) and a non-reactive tracer to measure dilution rate (hexafluorobenzene) were added and allowed to become well-mixed. Oxidant was introduced as ozone (~350 ppb) or HONO (50 ppb) in the presence of ultraviolet light (300–400 nm) to produce OH radicals. Multigenerational oxidation was initiated 4.5 h after initial oxidation, through the introduction of ~2 ppb min^{-1} HONO in the presence of ultraviolet light. Reactions were carried out at 20 °C and low relative humidity (<5%). All data are corrected for dilution due to instrument sampling. Reported particle mass concentrations were corrected for loss to the walls using a rate calculated from the loss rate of seed particles before reaction. Additional details are provided in Supplementary Section 1.

Measurements. Detailed operating conditions and calibration methods are provided for all instruments in Supplementary Section 1. Four high-resolution ($m/\Delta m \approx 4{,}000$) time-of-flight mass spectrometers (HTOF; Tofwerk AG) were used in this work: gas-phase composition was measured by PTR-MS[19,20] (Ionikon Analytik) and two CIMS[21] (Aerodyne Research) using I^- and NO_3^- as reagent ions[22–25], and particle-phase composition was measured by an AMS[18] (Aerodyne Research). The AMS sampled downstream of a TD[59] to measure the volatility distribution of particles. Two TILDAS[60] (Aerodyne Research) instruments measured C_1 compounds. Particle size distributions measured by Scanning Mobility Particle Sizer (TSI) were converted to mass concentration using an assumed density of 1.4 g cm^{-3}, and converted to carbon concentration via AMS-measured O:C and H:C ratios[61]. pOC was characterized by average properties of TD-AMS volatility bins. Particle-phase composition was also measured by the I^- CIMS using a 'FIGAERO' inlet. Owing to decomposition during thermal desorption, this instrument is also limited to characterization of pOC by average properties, which are found to be similar to measurements by AMS in concentration, elemental composition, carbon number and volatility. All pOC data shown in Figs. 1–4 are consequently from TD-AMS, as it has higher time resolution and lower uncertainty[62]. Further detail on pOC composition is discussed in Supplementary Sections 2 and 4. Calibration and data analysis was performed where possible through previously published techniques and with commercially available software. Detailed information regarding the comprehensive calibration of I^- CIMS data, and identification and quantification of species in PTR-MS data are described in Supplementary Sections 2 and 3.

Calculation of chemical parameters. Gas-phase mass spectrometers measure individual ions with a known molecular formula, while the TD-AMS provides bulk measurements of chemical properties. To explore chemical evolution, volatility was inferred from molecular composition and vice versa based on the approach in ref. [31], which relates c^* to n_C and elemental ratios (for example, those measured by the AMS). $\overline{OS_C}$ is calculated from elemental ratios[42].

Lifetime against atmospheric oxidation for a compound, i, was calculated from its rate constant for reaction with OH as $\tau_{ox,i} = (k_{OH,i}[\overline{OH}])^{-1}$ assuming an average OH concentration of 2×10^6 molecules cm^{-3}: OH rate constants for known compounds (those labelled in Figs. 1 and 2) were obtained from the National Institute of Standards and Technology Chemical Kinetics Database[44]. Rate constants for unidentified ions were calculated from molecular formula as described in ref. [45], and span an atmospheric lifetime of 13 h for small (high volatility) gases to ~2 h for larger, lower-volatility (for example, IVOC) gases. Lifetime of unmeasured mass is estimated from its time dependence (~4 h, Supplementary Fig. 9). Carbon is assumed to be lost from the particle phase with a lifetime of 69 d, as determined in ref. [46]; the conclusions in this study are insensitive to uncertainties in this value.

Uncertainty in carbon closure. Most uncertainties in all instrument calibrations introduce random error, not bias. Total uncertainty is consequently calculated by adding in quadrature the absolute uncertainty in each ion concentration. Relative uncertainty in total measured carbon is thus lower than the relative uncertainty of any given ion. Instrument and total uncertainties are provided in Supplementary Tables 1 and 2. The largest source of uncertainty in the total measured concentration is in the calibration of the I^- CIMS, which in this work is ~60% for its total carbon concentration (see Supplementary Section 4), though expected to be reduced to 20% in future work. The other main source of uncertainty in this work is the predicted bias in PTR measurements caused by the loss of carbon as neutral fragments in the mass spectrometer. Spectra of oxygenated and non-oxygenated compounds previously published and measured as part of this study demonstrate that compounds containing more than a few carbon atoms can lose 20% of their carbon as neutral fragments leading to potential underestimation and asymmetry in uncertainty estimates (see Supplementary Section 3). Fragmentation during analysis is also expected to bias the chemical characterization of the product mixture towards ions with lower carbon numbers. This bias cannot explain the observed decrease in n_C, as this trend is also observed in the I^- CIMS, which does not undergo increased fragmentation of more oxidized ions. The contribution of each instrument to total uncertainty in measured carbon is weighted by the fraction of carbon measured, which mitigates the relatively high uncertainty in I^- CIMS calibration due to its minority contribution to total measured carbon. The uncertainty in total carbon contributed by each instrument is: ±16% from I^- CIMS, ±1% from NO_3^- CIMS, $^{+11}_{-7}$% from PTR-MS, ±1% from TILDAS and ±3% from AMS/SMPS. Overall uncertainty in total measured carbon is ±20%; details provided in Supplementary Table 1.

Carbon closure is not substantially impacted by overlap between carbon measured by multiple instruments. The estimated overlap is 20 ppb C, which accounts for known possible transformations in instruments (for example, dehydration in the PTR-MS). Though not all possible transformations are well known or constrained, this estimate of multiply measured carbon is likely an overestimate in that it does not consider time dependence of ions; even ions measured by multiple instruments that do not correlate, which would represent different isomers, are included in the reported overlap.

Gas–particle–wall partitioning. Deposition of vapours to the walls was modelled as equilibrium gas–particle–wall partitioning of the observed carbon volatility distribution using parameters to match the conditions of these experiments, using a similar approach to that in ref. [63]. Briefly, the fraction of a volatility bin expected to be on the wall was modelled as a function of equilibration time, with parameterized competition between gas–wall partitioning, gas–particle partitioning, and reaction with OH to form a gas-phase product that does not partition. Time evolution of carbon on walls was simulated by modelled phase partitioning of the observed time-evolving volatility distribution of carbon. Details of these calculations are provided in Supplementary Section 4.

Data availability. A list of all ions measured in this work are provided in Supplementary Data 1. Time-resolved concentrations of all ions throughout the photooxidation and ozonolysis experiments (shown in Figs. 1 and 2, forming the basis for Figs. 3 and 4) are available from the corresponding authors on request.

Received: 19 May 2017; Accepted: 3 January 2018;
Published online: 26 February 2018

References

1. Sillman, S. The relation between ozone, NO_x and hydrocarbons in urban and polluted rural environments. *Atmos. Environ.* **33**, 1821–1845 (1999).
2. Atkinson, R. Atmospheric chemistry of VOCs and NO_x. *Atmos. Environ.* **34**, 2063–2101 (2000).
3. Lelieveld, J., Gromov, S., Pozzer, A. & Taraborrelli, D. Global tropospheric hydroxyl distribution, budget and reactivity. *Atmos. Chem. Phys.* **16**, 12477–12493 (2016).
4. Yang, Y. et al. Towards a quantitative understanding of total OH reactivity: a review. *Atmos. Environ.* **134**, 147–161 (2016).
5. Zhang, Q. et al. Ubiquity and dominance of oxygenated species in organic aerosols in anthropogenically-influenced Northern Hemisphere midlatitudes. *Geophys. Res. Lett.* **34**, L13801 (2007).
6. Jimenez, J.-L. et al. Evolution of organic aerosols in the atmosphere. *Science* **326**, 1525–1529 (2009).
7. Aumont, B., Szopa, S. & Madronich, S. Modelling the evolution of organic carbon during its gas-phase tropospheric oxidation: development of an explicit model based on a self generating approach. *Atmos. Chem. Phys.* **5**, 24975–2517 (2005).
8. Kroll, J. H. & Seinfeld, J. H. Chemistry of secondary organic aerosol: formation and evolution of low-volatility organics in the atmosphere. *Atmos. Environ.* **42**, 3593–3624 (2008).
9. Cappa, C. D. & Wilson, K. R. Multi-generation gas-phase oxidation, equilibrium partitioning, and the formation and evolution of secondary organic aerosol. *Atmos. Chem. Phys.* **12**, 9505–9528 (2012).
10. Donahue, N. M., Epstein, S. A., Pandis, S. N. & Robinson, A. L. A two-dimensional volatility basis set: 1. organic-aerosol mixing thermodynamics. *Atmos. Chem. Phys.* **11**, 3303–3318 (2011).
11. Goldstein, A. H. & Galbally, I. Known and unexplored organic constituents in the Earth's atmosphere. *Environ. Sci. Technol.* **41**, 1514–1521 (2007).
12. Calvert, J. G., Derwent, R. G., Orlando, J. J., Tyndall, G. S. & Wallington, T. J. *Mechanisms of Atmospheric Oxidation of the Alkanes* (Oxford Univ. Press, Oxford, 2007).
13. Lee, A. et al. Gas-phase products and secondary aerosol yields from the photooxidation of 16 different terpenes. *J. Geophys. Res. Atmos.* **111**, D17305 (2006).
14. Lee, A. et al. Gas-phase products and secondary aerosol yields from the ozonolysis of ten different terpenes. *J. Geophys. Res. Atmos.* **111**, D07302 (2006).
15. Zhang, X. et al. Influence of vapor wall loss in laboratory chambers on yields of secondary organic aerosol. *Proc. Natl Acad. Sci. USA* **111**, 5802–5807 (2014).
16. Robinson, A. L. et al. Rethinking organic aerosols: semivolatile emissions and photochemical aging. *Science* **315**, 1259–1262 (2007).
17. Isaacman-VanWertz, G. et al. Using advanced mass spectrometry techniques to fully characterize atmospheric organic carbon: current capabilities and remaining gaps. *Faraday Discuss.* **200**, 579–598 (2017).
18. Decarlo, P. F. et al. Field-deployable, high-resolution, time-of-flight aerosol mass spectrometer. *Anal. Chem.* **78**, 8281–8289 (2006).
19. Graus, M., Müller, M. & Hansel, A. High resolution PTR-TOF: quantification and formula confirmation of VOC in real time. *J. Am. Soc. Mass Spectrom.* **21**, 1037–1044 (2010).
20. Jordan, A. et al. A high resolution and high sensitivity proton-transfer-reaction time-of-flight mass spectrometer (PTR-TOF-MS). *Int. J. Mass Spectrom.* **286**, 122–128 (2009).
21. Aljawhary, D., Lee, A. K. Y. & Abbatt, J. P. D. High-resolution chemical ionization mass spectrometry (ToF-CIMS): application to study SOA composition and processing. *Atmos. Meas. Tech.* **6**, 3211–3224 (2013).
22. Jokinen, T. et al. Atmospheric sulphuric acid and neutral cluster measurements using CI-APi-TOF. *Atmos. Chem. Phys.* **12**, 4117–4125 (2012).

23. Krechmer, J. E. et al. Formation of low volatility organic compounds and secondary organic aerosol from isoprene hydroxyhydroperoxide low-NO oxidation. *Environ. Sci. Technol.* **49**, 10330–10339 (2015).
24. Lee, B. H. et al. An iodide-adduct high-resolution time-of-flight chemical-ionization mass spectrometer: application to atmospheric inorganic and organic compounds. *Environ. Sci. Technol.* **48**, 6309–6317 (2014).
25. Lopez-Hilfiker, F. D. et al. Constraining the sensitivity of iodide adduct chemical ionization mass spectrometry to multifunctional organic molecules using the collision limit and thermodynamic stability of iodide ion adducts. *Atmos. Meas. Tech.* **9**, 1505–1512 (2016).
26. Eddingsaas, N. C. et al. α-Pinene photooxidation under controlled chemical conditions—Part 1: gas-phase composition in low-and high-NO_x environments. *Atmos. Chem. Phys.* **12**, 6489–6504 (2012).
27. Capouet, M., Peeters, J., Nozière, B. & Müller, J.-F. Alpha-pinene oxidation by OH: simulations of laboratory experiments. *Atmos. Chem. Phys. Discuss* **4**, 4039–4103 (2004).
28. Pathak, R. K., Stanier, C. O., Donahue, N. M. & Pandis, S. N. Ozonolysis of α-pinene at atmospherically relevant concentrations: temperature dependence of aerosol mass fractions (yields). *J. Geophys. Res. Atmos.* **112**, D03201 (2007).
29. Donahue, N. M. et al. Aging of biogenic secondary organic aerosol via gas-phase OH radical reactions. *Proc. Natl Acad. Sci. USA* **109**, 13503–13508 (2012).
30. Hatakeyama, S., Ohno, M., Weng, J., Takagi, H. & Akimoto, H. Mechanism for the formation of gaseous and particulate products from ozone-cycloalkene reactions in air. *Environ. Sci. Technol.* **21**, 52–57 (1987).
31. Daumit, K. E., Kessler, S. H. & Kroll, J. H. Average chemical properties and potential formation pathways of highly oxidized organic aerosol. *Faraday Discuss.* **165**, 181–202 (2013).
32. Ehn, M. et al. A large source of low-volatility secondary organic aerosol. *Nature* **506**, 476–479 (2014).
33. Ehn, M. et al. Composition and temporal behavior of ambient ions in the boreal forest. *Atmos. Chem. Phys.* **10**, 8513–8530 (2010).
34. Saunders, S. M., Jenkin, M. E., Derwent, R. G. & Pilling, M. J. Protocol for the development of the Master Chemical Mechanism, MCMv3 (Part A): tropospheric degradation of non-aromatic volatile organic compounds. *Atmos. Chem. Phys.* **3**, 161–180 (2003).
35. Worton, D. R., Gentner, D. R., Isaacman, G. & Goldstein, A. H. Embracing complexity: deciphering origins and transformations of atmospheric organics through speciated measurements. *Environ. Sci. Technol.* **46**, 5265–5266 (2012).
36. Nah, T. et al. Influence of seed aerosol surface area and oxidation rate on vapor wall deposition and SOA mass yields: a case study with α-pinene ozonolysis. *Atmos. Chem. Phys.* **16**, 9361–9379 (2016).
37. Trump, E. R., Epstein, S. A., Riipinen, I. & Donahue, N. M. Wall effects in smog chamber experiments: a model study. *Aerosol Sci. Technol.* **50**, 1180–1200 (2016).
38. Ye, P. et al. Vapor wall loss of semi-volatile organic compounds in a Teflon chamber. *Aerosol Sci. Technol.* **50**, 822–834 (2016).
39. Nozière, B., Barnes, I. & Becker, K.-H. Product study and mechanisms of the reactions of α-pinene and of pinonaldehyde with OH radicals. *J. Geophys. Res. Atmos.* **104**, 23645–23656 (1999).
40. Iyer, S., Lopez-Hilfiker, F. D., Lee, B. H., Thornton, J. A. & Kurtén, T. Modeling the detection of organic and inorganic compounds using iodide-based chemical ionization. *J. Phys. Chem. A* **120**, 576–587 (2016).
41. Pagonis, D., Krechmer, J. E., Gouw, J. De, Jimenez, J. L.& Ziemann, P. J. Effects of gas–wall partitioning in Teflon tubing and instrumentation on time-resolved measurements of gas-phase organic compounds. *Atmos. Meas. Tech.* **10**, 4687–4696 (2017).
42. Kroll, J. H. et al. Carbon oxidation state as a metric for describing the chemistry of atmospheric organic aerosol. *Nat. Chem.* **3**, 133–139 (2011).
43. Lee, B. H. et al. Highly functionalized organic nitrates in the southeast United States: contribution to secondary organic aerosol and reactive nitrogen budgets. *Proc. Natl Acad. Sci. USA* **113**, 1516–1521 (2016).
44. Manion, J. A. et al. *NIST Chemical KineticsDatabase, NIST Standard Reference Database 17* v.7.0 (web version), data v.2015.12 (National Institute of Standards and Technology, 2015); http://kinetics.nist.gov/kinetics/
45. Donahue, N. M. et al. Why do organic aerosols exist? Understanding aerosol lifetimes using the two-dimensional volatility basis set. *Environ. Chem.* **10**, 151–157 (2013).
46. Kroll, J. H., Lim, C. Y., Kessler, S. H. & Wilson, K. R. Heterogeneous oxidation of atmospheric organic aerosol: kinetics of changes to the amount and oxidation state of particle-phase organic carbon. *J. Phys. Chem. A* **119**, 10767–10783 (2015).
47. Dixon-Lewis, G. Flames structure and flame reaction kinetics VII. Reactions of traces of heavy water, deuterium and carbon dioxide added to rich hydrogen + nitrogen + oxygen flames. *Proc. R. Soc. London A* **330**, 219–245 (1972).
48. Raff, J. D., Stevens, P. S. & Hites, R. A. Relative rate and product studies of the OH–acetone reaction. *J. Phys. Chem. A* **108**, 4728–4735 (2005).
49. Richards-Henderson, N. K., Goldstein, A. H. & Wilson, K. R. Large enhancement in the heterogeneous oxidation rate of organic aerosols by hydroxyl radicals in the presence of nitric oxide. *J. Phys. Chem. Lett.* **6**, 4451–4455 (2015).
50. Paulot, F. et al. Unexpected epoxide formation in the gas-phase photooxidation of isoprene. *Science* **325**, 730–733 (2013).
51. Surratt, J. D. et al. Reactive intermediates revealed in secondary organic aerosol formation from isoprene. *Proc. Natl Acad. Sci. USA* **107**, 6640–6645 (2010).
52. Palm, B. B. et al. In situ secondary organic aerosol formation from ambient pine forest air using an oxidation flow reactor. *Atmos. Chem. Phys.* **16**, 2943–2970 (2016).
53. Chan, A. W. H. et al. Speciated measurements of semivolatile and intermediate volatility organic compounds (S/IVOCs) in a pine forest during BEACHON-RoMBAS 2011. *Atmos. Chem. Phys.* **16**, 1187–1205 (2016).
54. Tkacik, D. S., Presto, A. A., Donahue, N. M. & Robinson, A. L. Secondary organic aerosol formation from intermediate-volatility organic compounds: cyclic, linear, and branched alkanes. *Environ. Sci. Technol.* **46**, 8773–8781 (2012).
55. Park, J.-H. et al. Active atmosphere–ecosystem exchange of the vast majority of detected volatile organic compounds. *Science* **341**, 643–648 (2013).
56. Nguyen, T. B. et al. Rapid deposition of oxidized biogenic compounds to a temperate forest. *Proc. Natl Acad. Sci. USA* **112**, E392–E401 (2015).
57. Wolfe, G. M. et al. Formaldehyde production from isoprene oxidation across NO_x regimes. *Atmos. Chem. Phys.* **16**, 2597–2610 (2016).
58. Warneke, C. et al. Photochemical aging of volatile organic compounds in the Los Angeles basin: weekday–weekend effect. *J. Geophys. Res. Atmos.* **118**, 5018–5028 (2013).
59. Faulhaber, A. E. et al. Characterization of a thermodenuder-particle beam mass spectrometer system for the study of organic aerosol volatility and composition. *Atmos. Meas. Tech.* **2**, 15–31 (2009).
60. McManus, J. B. et al. Pulsed quantum cascade laser instrument with compact design for rapid, high sensitivity measurements of trace gases in air. *Appl. Phys. B Lasers Opt.* **92**, 387–392 (2008).
61. Canagaratna, M. R. et al. Elemental ratio measurements of organic compounds using aerosol mass spectrometry: characterization, improved calibration, and implications. *Atmos. Chem. Phys.* **15**, 253–272 (2015).
62. Lopez-Hilfiker, F. D. et al. A novel method for online analysis of gas and particle composition: description and evaluation of a filter inlet for gases and AEROsols (FIGAERO). *Atmos. Meas. Tech.* **7**, 983–1001 (2014).
63. La, Y. S. et al. Impact of chamber wall loss of gaseous organic compounds on secondary organic aerosol formation: explicit modeling of SOA formation from alkane and alkene oxidation. *Atmos. Chem. Phys.* **16**, 1417–1431 (2016).

Acknowledgements

We thank H. Stark for insights into correcting for mass-dependent transmission in the I^- CIMS calibration, J.-L. Jimenez for valuable discussions regarding vapour wall loss, C. Heald for valuable discussions of overall chemical trends and L. Wattenberg for the inspiration for the stacked plot approach to visualizing these data. This work was supported in part by the National Science Foundation (NSF) Postdoctoral Research Fellowship programme (AGS-PRF 1433432), as well as grants AGS-1536939, AGS-1537446 and AGS-1536551. D.A.K. acknowledges support from NSF grant AGS-1446286.

Author contributions

Experiments were conducted by G.I.-V.W., P.M., R.O'B., C.L., J.B.N., J.P.F., P.K.M., C.A., L.S., D.A.K., A.T.L., J.R.R. and S.T.H., with data analysis by these researchers with significant contributions by J.A.M., J.F.H., A.H.G., T.B.O., M.R.C., J.H.K., J.T.J. and D.R.W. G.I.-V.W. and J.H.K. interpreted the results. The manuscript was prepared by G.I.-V.W. and J.H.K., with contributions and editing by all listed authors.

Competing interests

P.M., J.B.N., J.R.R., S.T.H., T.B.O., M.R.C., J.T.J. and D.R.W. are (or were during this work) employees of Aerodyne Research, Inc. (ARI), which developed and commercialized several of the advanced mass spectrometric instruments utilized in this study.

Additional information

Supplementary information is available for this paper at https://doi.org/10.1038/s41557-018-0002-2.

Reprints and permissions information is available at www.nature.com/reprints.

Correspondence and requests for materials should be addressed to G.I. or J.H.K.

Publisher's note: Springer Nature remains neutral with regard to jurisdictional claims in published maps and institutional affiliations.